JACS
JOURNAL OF THE AMERICAN CHEMICAL SOCIETY
Article
pubs.acs.org/JACS

Growth Intermediates for CVD Graphene on Cu(111): Carbon Clusters and Defective Graphene

Tianchao Niu,[†] Miao Zhou,[‡] Jialin Zhang,[‡] Yuanping Feng,[‡] and Wei Chen*[,†,‡]

[†]Department of Chemistry, National University of Singapore, 3 Science Drive 3, 117543, Singapore
[‡]Department of Physics, National University of Singapore, 2 Science Drive 3, 117542, Singapore

Supporting Information

ABSTRACT: Graphene growth on metal films via chemical vapor deposition (CVD) represents one of the most promising methods for graphene production. The realization of the wafer scale production of single crystalline graphene films requires an atomic scale understanding of the growth mechanism and the growth intermediates of CVD graphene on metal films. Here, we use *in situ* low-temperature scanning tunneling microscopy (LT-STM) to reveal the graphene growth intermediates at different stages via thermal decomposition of methane on Cu(111). We clearly demonstrate that various carbon clusters, including carbon dimers, carbon rectangles, and 'zigzag' and 'armchair'-like carbon chains, are the actual growth intermediates prior to the graphene formation. Upon the saturation of these carbon clusters, they can transform into defective graphene possessing pseudoperiodic corrugations and vacancies. These vacancy-defects can only be effectively healed in the presence of methane via high temperature annealing at 800 °C and result in the formation of vacancy-free monolayer graphene on Cu(111).

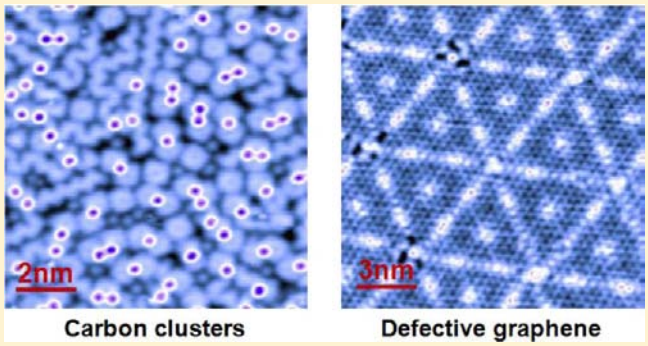

1. INTRODUCTION

Single-crystal graphene films are highly desirable for the development of high-performance graphene based devices.[1−4] Chemical vapor deposition (CVD) on transition metal surfaces represents a promising and scalable approach to achieve reasonably high-quality graphene for device application.[4−10] However, the formation of grain boundaries and structural defects during the synthesis process would significantly deteriorate the quality of graphene.[11−13] Previous studies have shown that the quality of as-grown graphene film dramatically depends on the structure, adsorption, and nucleation of carbon species at the initial stages on the metal surfaces during the CVD process.[14−17] Therefore, revealing the graphene growth mechanism at the atomic scale, as well as the graphene growth intermediates, is of paramount importance to realize the wafer scale production of single crystalline graphene films.

Intensive experimental and theoretical studies have been devoted to revealing the atomic structure of surface carbon species during the initial stages of CVD graphene grown on transition metal surfaces.[18−32] It is believed that carbon monomer and dimer species arising from hydrocarbon decomposition on metal surfaces are the primary intermediates prior to the formation of larger carbon clusters, which can further develop into single layer or multilayer graphene films.[18−20] A recent photoemission study clearly reveals the formation of carbon dimer species via thermal decomposition of ethene on Co(0001).[21] For larger carbon clusters, it has been proposed that chain configurations are much more energetically favorable than the sp^2 networks or graphene nanoflakes when the cluster size is below the critical size of $N = 12$.[22] It is also found that the five-carbon-atomic chain structure is one of the most important carbon intermediates on Ir(111) and Cu(111).[23] Combined STM and first principle calculations reveal that the intermediates in the initial stage of graphene grown on Rh(111) using ethane are the size-selective carbon clusters with 7 fused six-member-carbon-rings.[24] The same structure has also been found on the Ru(0001) surface.[25] From *ab initio* calculations, core−shell structured C_{21} with a carbon hexagon surrounded by five carbon pentagons is found to be the most stable magic cluster on the Ru(0001), Ni(111), and Cu(111).[26]

Cu films have been widely used for CVD growth of graphene.[1,8,33−39] The Cu(111) facet has been proposed to be the ideal surface to produce uniform high-quality monolayer graphene.[37−39] Although the formation of carbon dimers,[18−20] atomic-carbon nanoarches,[29,30] and a magic C_{21} carbon cluster[26] in the graphene grown on Cu have been theoretically proposed, experimental investigations on the surface intermediates for CVD graphene growth on Cu is very limited.[34−36] In this regard, the experimental investigation of the surface intermediates at different stages of graphene growth on Cu(111) would be of great interest.

Received: April 10, 2013
Published: May 15, 2013

   dx.doi.org/10.1021/ja403583s | *J. Am. Chem. Soc.* 2013, 135, 8409−8414

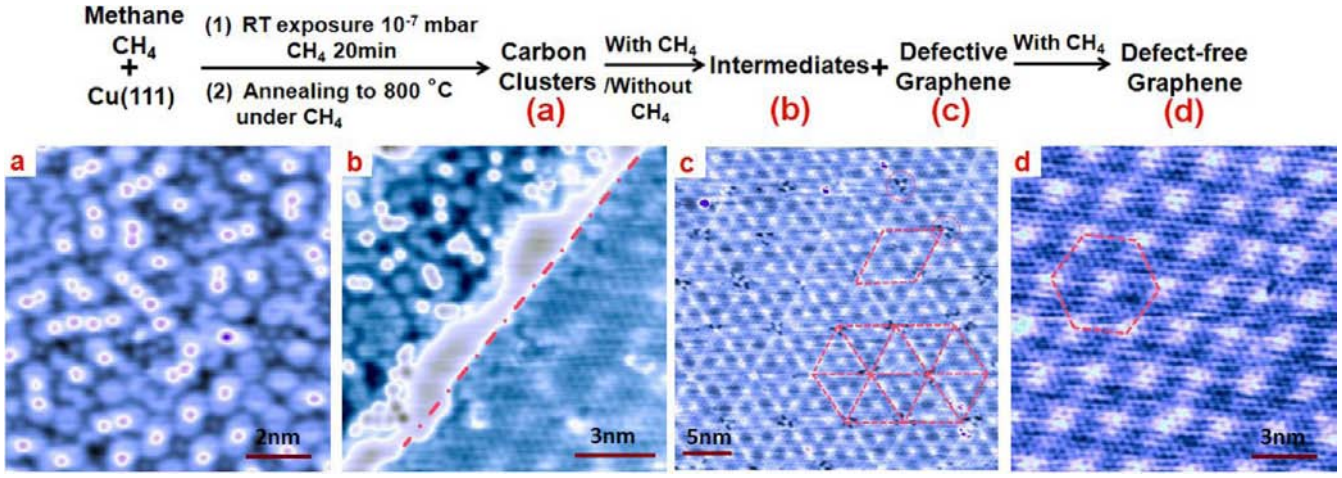

Figure 1. Evolution of graphene grown via thermal decomposition of methane on Cu(111). *Top*: Schematic illustration of the surface intermediates at different reaction conditions. *Bottom*: overview of STM images showing (a) carbon clusters, (b) the boundary between carbon cluster (left) and defective graphene (right), (c) defective graphene, and (d) vacancy-free graphene, at different reaction stages. Scanning parameters: (a) V_{tip} = 0.8 V, I = 80 pA; (b) V_{tip} = 0.6 V, I = 100 pA; (c) V_{tip} = 0.2 V, I = 90 pA; (d) V_{tip} = 0.5 V, I = 90 pA.

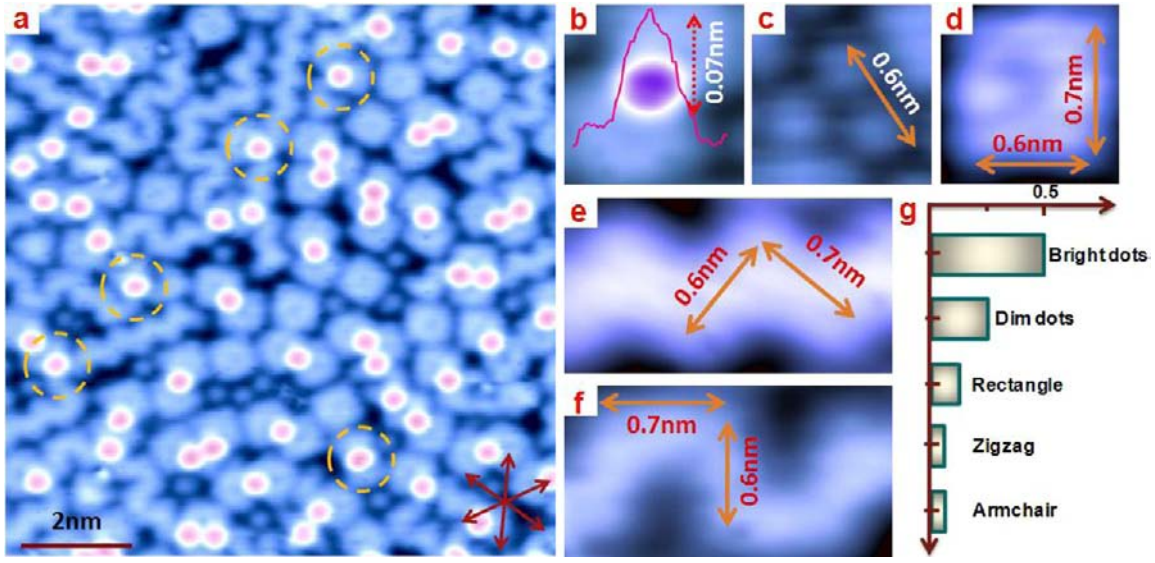

Figure 2. Carbon clusters on Cu(111). (a) STM image showing a Cu(111) terrace fully decorated by carbon clusters. Inset shows the high-symmetry directions of Cu(111). (b–f) Enlarged STM images showing five types of carbon clusters coexisting on the Cu(111) surface: (b) the bright dot at the joint of two large clusters; (c) dim dots; (d) carbon rectangles; (e) zigzag-like; and (f) armchair-like carbon chains. (g) Histogram shows the relative ratio of the carbon clusters. The parallel axis shows the number of carbon clusters per nm^2. Scanning parameters: (a) V_{tip} = 0.6 V, I = 100 pA. (b–f): V_{tip} = 0.6 V, I = 200 pA.

Here, we report an atomic scale investigation of the growth intermediates of CVD graphene on Cu(111) at the different growth stages using methane as precursor, through the combination of *in situ* low-temperature scanning tunneling microscopy (LT-STM) experiments and theoretical calculations. Prior to the graphene formation, methane decomposed into various carbon clusters decorated on Cu(111), comprising carbon dimers, carbon rectangles, and 'zigzag' and 'armchair'-like carbon chains. Upon the saturation of these carbon clusters on Cu(111), they transformed into defective graphene by repeating the methane exposing and annealing cycles. The defective graphene possesses pseudoperiodic corrugations and point defects (vacancies). It is found that the defects in the defective graphene can only be healed via high temperature annealing in the presence of methane at 800 °C, resulting in the formation of vacancy-free single layer graphene on Cu(111).

2. RESULTS AND DISCUSSION

2.1. Overview of the Evolution of CVD Graphene on Cu(111). The graphene was grown via thermal decomposition of methane (CH_4, partial pressure of 10^{-7} mbar) on the clean Cu(111) at 800 °C in an ultrahigh vacuum chamber (UHV, see details in Methods). Figure 1 summarizes the key surface carbon species at different stages during graphene evolution on Cu(111). As shown in Figure 1a, after exposed to CH_4 at room temperature (RT) followed by sequential annealing up to 800 °C in UHV, the Cu(111) was almost fully decorated with various carbon clusters, comprising carbon dimers, carbon rectangles, and 'armchair' and 'zigzag'-like carbon chains (details will be discussed in section 2.2). At this stage, we did not observe the formation of graphene flakes on Cu(111). It is worthy to mention that the direct exposure of CH_4 to Cu(111) at 800 °C cannot give rise to carbon cluster formation. This

dx.doi.org/10.1021/ja403583s | J. Am. Chem. Soc. 2013, 135, 8409–8414

suggests that RT adsorption of CH_4 on Cu(111) is very critical for the CH_4 decomposition and the carbon cluster formation.[36] Further annealing these carbon cluster either in the presence or in the absence of CH_4 can lead to the transformation to defective graphene on Cu(111). Figure 1b highlights this transition stage, clearly showing a boundary between the defective graphene and the carbon clusters. Such a boundary, i.e., a bright island with no distinctive features, can be identified as the transition intermediates from carbon clusters to defective graphene. It is found that the domain size of individual defective graphene and its coverage on Cu(111) increased progressively with the thermal annealing cycles. As highlighted in Figure 1c, the defective graphene possessed pseudoperiodic corrugations with vacancies formed at the vertex. These defects (vacancies) can only be healed via high temperature annealing in the presence of CH_4 at 800 °C, leading to formation of vacancy-free monolayer graphene (Figure 1d).

2.2. Carbon Clusters. Figure 2a shows a typical STM image for Cu(111) fully decorated with various carbon clusters, comprising bright and dim dots (Figure 2b and c), carbon rectangles (Figure 2d), 'zigzag'-like chains (Figure 2e), and 'armchair'-like chains (Figure 2f). The distribution of these five types of carbon clusters on Cu(111) is summarized in the histogram in Figure 2g.

The population of the bright dots is nearly twice that of the dim ones, while their sizes are almost identical at ~0.3 nm, as shown in Figure 2a, b, and c. Moreover, the bright dots predominantly located at the joints of the large carbon clusters (Figure 2a and the enlarged STM image of Figure 2b), while the dim dots dispersed on Cu(111) surface. As seen from the bias-dependent STM images (Figure S1 in Supporting Information), the STM topography size of these dots is comparable to that of the acetylene (C_2H_2) on Cu(111)[40] or Cu(110)[41] (~0.40 nm), but significantly smaller than that of single benzene molecule on Cu(111) (~0.60 nm).[42] Previous theoretical calculations have also reported that the carbon dimers are energetically favorable on Cu(111) surface.[18−20] As such, we assign the observed bright and dim dots to carbon dimers (C_2H_x).

By carefully scrutinizing the enlarged STM images of the three types of large carbon clusters (Figure 2d−f), all these carbon clusters possess the same basic building block composed of two perpendicular lobes with the length of ~0.60 nm and ~0.70 nm, respectively. As shown in Figure 2a and d−f, the carbon rectangles are closed systems and hence can be isolated from other clusters, while the 'zigzag' and 'armchair'-like carbon chains are open systems, and hence they tend to form longer chains to stabilize the structures. Those smaller clusters consisting of one basic building block were joined through the bright dots (carbon dimers) as highlighted by the yellow dashed circles in Figure 2a. These bright dots can also serve as joints to connect other larger clusters. It is worth mentioning that the formation of stable carbon fragments is governed by the interplay between the C−C bond formation and the interaction of carbon atoms with the metal substrate.[20] The Cu(111) substrate can strongly influence structural alignment of these carbon clusters as well as their atomic structures prior to the formation of larger graphitic flakes.[19] As shown in Figure 3a, the alignment of these carbon clusters with respect to Cu(111) substrate can be distinctly identified. For example, the short side of the carbon rectangles predominantly aligned along the close-packed ⟨1−10⟩ direction; while the long side aligned along the ⟨11−2⟩ direction of Cu(111).

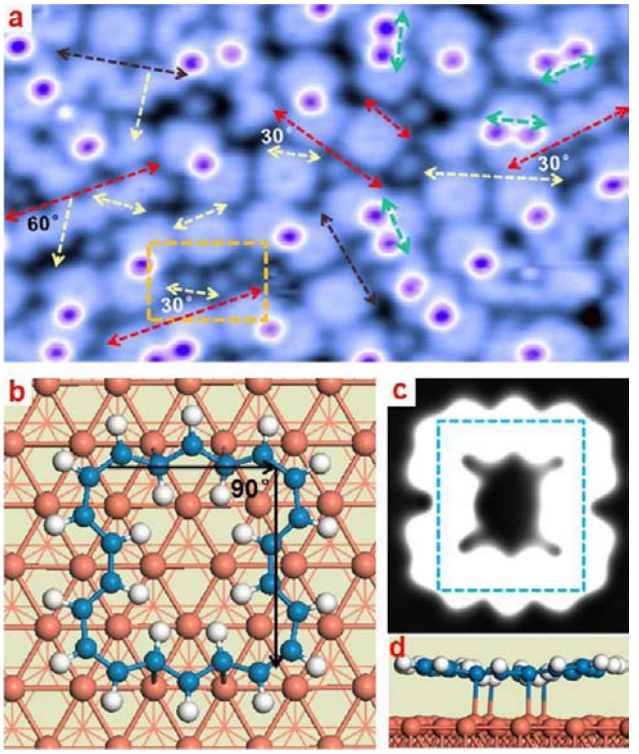

Figure 3. (a) STM image showing the ordered alignment of the carbon clusters with respect to the substrate lattice. The red arrows indicate the high-symmetry directions of Cu(111), and light yellow and dark red arrows highlight the orientation of the clusters. (b) Optimized structure of the carbon rectangle on Cu(111), and (d) the corresponding side view; (c) simulated STM image of the carbon rectangle. Scanning parameters: (a) V_{tip} = 0.6 V, I = 100 pA.

We carried out first-principle density-functional-theory (DFT) calculations to propose and understand the atomic structures of these large carbon clusters (i.e., carbon rectangles, 'zigzag' and 'armchair'-like carbon chains) on Cu(111) (details, see Methods). As mentioned before, all three carbon clusters possess the same basic building block. Therefore, we chose the closed system of carbon rectangle as an example to perform detailed DFT calculations. Previous studies reported that partially dehydrogenated carbon species are the intermediates for methane dissociation on transition metal surfaces.[43,44] It is also found that partially dehydrogenated CH_x is energetically favorable at the initial stages before the transformation into larger clusters.[19] Therefore, several partially dehydrogenated structures were proposed and optimized via DFT calculations. We found that carbon chain with the −CH unit was the most energetically favorable. Figure 3b presented the optimized structure for the carbon rectangle cluster with an average carbon bond length of 1.42 Å ($C_{22}H_{22}$). As seen from the side view of the carbon cluster (Figure 3d), four C−Cu bonds at the middle of the 'zigzag'-like chain can be recognized. As shown in Figure 3b, the 'zigzag' and 'armchair'-like chains aligned exactly along the ⟨1−10⟩ and ⟨11−2⟩ directions of Cu(111) with a length of 0.63 and 0.71 nm, respectively. Figure 3c displays the simulated STM image of this proposed carbon rectangle, in good agreement with the experimental STM results.

Our atomic scale investigation at the initial stage of graphene evolution on Cu(111) clearly reveals the presence of various partially dehydrogenated carbon clusters as surface intermediates for CVD graphene growth on Cu(111). The results are

dx.doi.org/10.1021/ja403583s | J. Am. Chem. Soc. 2013, 135, 8409−8414

consistent with a recent study of molecular dynamics (MD) simulation of methane decomposition on Cu(111).[19] The saturation of these clusters resulted in the transformation into defective graphene (Figure 1b,c). We analyzed the relative ratio of various carbon clusters at different regions at this transition stage, such as on the terraces fully decorated by the carbon clusters, and the cluster regions adjacent to the defective graphene. Interestingly, we did not observe any apparent change of the relative ratios of these carbon clusters at different regions (Figure S2 in Supporting Information). This suggests that all these carbon clusters participated into the transformation into defective graphene (Figure S2 in Supporting Information).

2.3. Defective Graphene. The STM topography image and the corresponding conductance map of the defective graphene on Cu(111) are shown in Figure 4a and b,

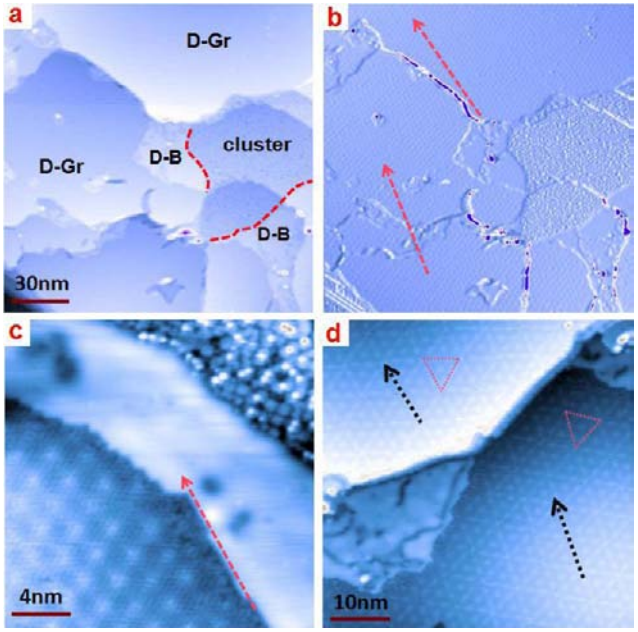

Figure 4. (a) STM topography image of ~0.8 monolayer of defective graphene (D-Gr) on Cu(111), and (b) the corresponding conductance image recorded simultaneously with the STM image of (a). (c) Domain boundary (D-B, intermediates) between the carbon clusters and defective graphene. (d) Defective graphene on neighboring two terraces isolated by the Cu step, where the black dashed arrows highlighted the direction of the high-symmetry moiré spots with an angle of ~13° with respect to each other. D-Gr denotes defective graphene, and D-B Domain boundary. Scanning parameters: (a) V_{tip} = 2.1 V, I = 86 pA; (c) and (d) V_{tip} = 0.6 V, I = 90 pA.

respectively. Clearly, on each terrace, we did not observe the appearance of multidomains of defective graphene. This means that each Cu(111) terrace can be covered by one single domain of defective graphene. Figure 4c displays the region with the coexistence of defective graphene and carbon clusters. The domain boundaries (DB) between the defective graphene and carbon clusters appeared as bright islands without prominent atomic features. These domain boundaries can only be observed on the terrace of Cu(111), rather than at the step edges, as seen from Figure 4a and Figure S2 in Supporting Information. The domain size and the total coverage of defective graphene increased with the thermal annealing cycles. Figure 4d shows STM topography of defective graphene on two separated terraces. Each terrace was completely covered by a single domain of defective graphene with identical moiré periodic. However, the in-plane orientations of both moiré patterns differed from each other by an angle of ~13° as indicated by the dashed arrows.

Figure 5a shows a typical atomically resolved STM image of defective graphene possessing pseudoperiodic corrugations and

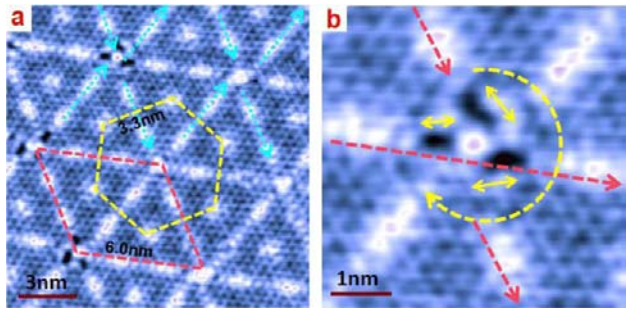

Figure 5. Striking features of the defective graphene on Cu(111). (a) High-resolution STM image of the defective graphene with pseudoperiodic corrugations, where the yellow hexagon represented the nearest neighboring vacancy-free moiré spots, and the green arrows indicated the misfit of the corrugations. (b) STM image showing a typical vacancies at the intersection of the pseudoperiodic corrugations. Scanning parameters: (a) V_{tip} = 0.2 V, I = 90 pA; (b) V_{tip} = 0.1 V, I = 100 pA.

vacancies (i.e., missing carbon atoms) at the vertex (dark holes). The diamond in Figure 5a highlights the 'unit cell' of the defective graphene with the dimension of ~6.0 nm. Dislocations and vacancies were regularly observed at the vertex of the diamonds as guided by the green arrows (Figure 5a). The vacancy-free moiré spots can only be formed at the center of each triangle with an average distance of ~3.3 nm as indicated by the yellow hexagon. Close inspection of the typical vacancies (Figure 5b) reveals that these vacancies formed at the corrugation intersections and arose from the misfit of the corrugations. It is also found that three vacancies located alternately at the intersection of the corrugations (also can be seen in Figure 1c). We propose that the formation of these vacancy defects can help release the interfacial stress due to the lattice mismatch between graphene and Cu(111) at the initial growth stage of graphene on Cu(111).[33] Moreover, the defective graphene possesses pseudo-ordered point defects (vacancies). This can be an alternative route to the defect creation in graphene and hence to engineer the graphene properties or functionalities, in addition to the traditional methods, like electron beam irradiation or Ar^+ ion bombardment to create defects in graphene.[45−47]

2.4. Defects Healing to Form Vacancy-Free Monolayer Graphene on Cu(111). Annealing the defective graphene at 800 °C in the presence of methane can heal those vacancies in defective graphene, leading to the formation of vacancy-free monolayer graphene on Cu(111), as shown in Figure 1d and Figure 6a. We have to stress that annealing the defective graphene in the absence of methane cannot give rise to the formation of the vacancy-free graphene. This phenomenon differs from the previously reported self-healing[48,49] or substrate assisted healing of graphene defects in the absence of carbon feedstock.[50,51] In our experiments, methane played an essential role to serve as both carbon source and defect healer.

dx.doi.org/10.1021/ja403583s | J. Am. Chem. Soc. 2013, 135, 8409−8414

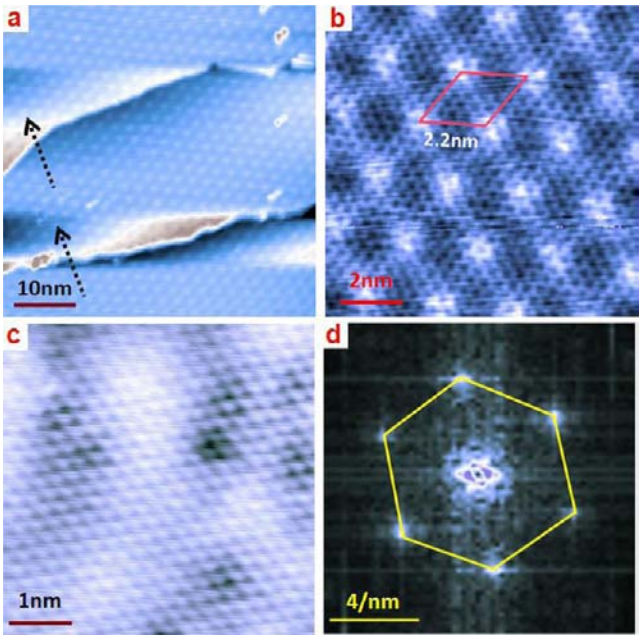

Figure 6. (a) STM image showing the vacancy-free graphene after healing at 800 °C in the presence of methane gas, where the dashed arrows indicate the direction of high symmetry moiré pattern. (b) Enlarged STM image showing the moiré periodicity of ~2.2 nm; (c) atomic resolution STM image; and (d) its corresponding FFT showing the 1 × 1 graphene lattice. Scanning parameters: (a) V_{tip} = 2.0 V, I = 100 pA; (b) V_{tip} = 0.5 V, I = 100 pA; (c) V_{tip}= 0.1 mV, I = 90 pA.

The arrows in Figure 6a indicated the direction of the high symmetry moiré pattern overcrossing the Cu steps with a moiré periodicity of ~2.2 nm (Figure 6b). Moreover, a $\sqrt{3} \times \sqrt{3}$ modulation of the vacancy-free graphene on Cu(111) can be observed under a tip bias range above 10 mV and below −10 mV (see details in Supporting Information Figure S3). Atomic-resolution STM image in Figure 6c clearly shows the hexagonal lattice of the vacancy-free graphene on Cu(111) with the lattice constant of about 0.25 nm as corroborated by its corresponding FFT image (Figure 6d). From the known moiré periodicity of 2.2 nm, we can calculate the misorientation angle between the vacancy-free graphene and Cu(111) to be 6.6°. The detailed calculation of the misorientation angle and the simulated moiré pattern of the vacancy-free graphene on Cu(111) can be found in Supporting Information Figure S4.

3. CONCLUSION

In summary, through the combination of in situ LT-STM experiments and DFT calculations, we revealed the growth intermediates of CVD graphene on Cu(111) via thermal decomposition of methane at different growth stages, comprising various carbon clusters (i.e., carbon dimers, carbon rectangles, 'zigzag' and 'armchair'-like carbon chains) and defective graphene. Saturation of these carbon clusters on Cu(111) resulted in the transformation into defective graphene possessing pseudo-ordered corrugations and vacancies due to lattice mismatching. These defects can only be healed by high temperature annealing in the presence of methane and transformed into vacancy-free single layer graphene. Such atomic insights of the structural evolution at different stages of graphene grown on Cu(111) can help better understand the growth mechanism of CVD graphene, and hence provide design rules for the large scale growth of single crystalline graphene films. Moreover, the growth of defective graphene with pseudo-ordered point defects (vacancies) can open up a new route for the controllable creation of defects and hence engineer the properties and functionalities of graphene.

4. METHODS

Growth of Graphene on Cu(111) in UHV Chamber at Different Stages. Cu(111) substrate was cleaned by several cycles of Ar+ ion bombardment (800 eV energy, 20 μA/cm^2 ion current density) and thermal annealing (40 min at 880 K). Cleanliness of the Cu(111) surface was checked by STM before CVD growth.[52] The methane (CH_4) gas was introduced into the UHV chamber through a leak valve, and the pressure was controlled to be 10^{-7}mbar, monitored by a cold cathode gauge. Different surface species can be generated in different repeated thermal cycles in a constant background pressure of methane. The Cu surface can be decorated with carbon clusters after two cycles, while defective graphene can be formed after the saturation of the carbon clusters. The coverage of defective graphene can be controlled by the number of thermal cycles. The defects can be healed by annealing in the presence of methane at 800 °C.

UHV LT-STM Experimental Details. STM measurements were performed in a custom built multichamber STM system with base pressure better than 1.0 × 10^{-10} mbar, housing an Omicron LT-STM interfaced to a Nanonis controller.[53] The CVD graphene was synthesized in the growth chamber. The as-grown sample was transferred to the STM chamber after cooling down to room temperature. All the STM images were measured at liquid nitrogen temperature (77 K) using the constant current mode and an electrochemically etched tungsten (W) tip.[52] The bias voltage was applied on the tip during the STM observation.

Modeling and Computational Details. A four-layer slab model with fixed bottom layer was used to test the configurations of carbon clusters. A supercell that consists of c (8 × 7) repeated Cu (111) slabs that were separated by a vacuum region of 20 Å was adopted. For the structure of the basic component, the number of bonded hydrogen atoms on the carbon backbone was optimized to show that each carbon atom bonded with one hydrogen atom is the most energetically favorable.

All theoretical calculation were carried out by a DFT[54,55] method implemented in the Vienna ab initio simulation package (VASP) with the projector augmented-wave (PAW) method and general gradient approximation (GGA) in Perdew–Burke–Ernzerhof (PBE) format with a kinetic energy cutoff of 400 eV.[56,57] All structures were optimized by a conjugate gradient method until the residual force component on each atom was less than 0.01 eV/Å. STM images were simulated within the Tersof-Hamman approximation.[58]

■ ASSOCIATED CONTENT

Ⓢ Supporting Information

Figure S1: Bias dependent STM images of the carbon clusters; Figure S2: Distribution of the carbon clusters on different regions; Figure S3: STM images of the $\sqrt{3}\times\sqrt{3}$ reconstructed graphene; Figure S4: Calculation of the moiré pattern. This material is available free of charge via the Internet at http://pubs.acs.org.

■ AUTHOR INFORMATION

Corresponding Author

phycw@nus.edu.sg

Notes

The authors declare no competing financial interest.

■ ACKNOWLEDGMENTS

Authors acknowledge the support from Singapore MOE grants R143-000-505-112, R143-000-530-112, R143-000-542-112, and

NUS YIA grant R143-000-452-101. We thank Z. Y. Luo, F. Pan, and S. L. Wong for helpful discussion.

REFERENCES

(1) Li, X. S.; Magnuson, C. W.; Venugopal, A.; Tromp, R. M.; Hannon, J. B.; Vogel, E. M.; Colombo, L.; Ruoff, R. S. *J. Am. Chem. Soc.* **2011**, *133*, 2816.
(2) Bae, S. K.; Kim, H.; Lee, Y. B.; Xu, X. F.; Park, J. S.; Zheng, Y.; Balakrishnan, J.; Lei, T.; Kim, H. R.; Song, Y.; Kim, Y. J.; Kim, K. S.; Özyilmaz, B.; Ahn, J. H.; Hong, B. H.; Iijima, S. *Nat. Nanotechnol.* **2010**, *5*, 574.
(3) Bhaviripudi, S.; Jia, X. T.; Dresselhaus, M. S.; Kong, J. *Nano Lett.* **2010**, *10*, 4128.
(4) Edwards, R. S.; Coleman, K. S. *Acc. Chem. Res.* **2013**, *46*, 23.
(5) Sun, Z. Z.; Yan, Z.; Yao, J.; Beitler, E.; Zhu, Y.; Tour, J. M. *Nature* **2010**, *468*, 549.
(6) Kim, K. S.; Zhao, Y.; Jang, H.; Lee, S. Y.; Kim, J. M.; Kim, K. S.; Ahn, J. H.; Kim, P.; Choi, J. Y.; Hong, B. H. *Nature* **2009**, *457*, 706.
(7) Dai, B. Y.; Fu, L.; Zou, Z. Y.; Wang, M.; Xu, H. T.; Wang, S.; Liu, Z. F. *Nat. Commun.* **2011**, *2*, 522.
(8) Geng, D. C.; Wu, B.; Guo, Y. L.; Huang, L. P.; Xue, Y. Z.; Chen, J. Y.; Yu, G.; Jiang, L.; Hu, W. P.; Liu, Y. Q. *Proc. Natl. Acad. Sci. U.S.A.* **2012**, *109*, 7992.
(9) Gao, L. B.; Ren, W. C.; Xu, H. L.; Jin, L.; Wang, Z. X.; Ma, T.; Ma, L. P.; Zhang, Z. Y.; Fu, Q.; Peng, L. M.; Bao, X. H.; Cheng, H. M. *Nat. Commun.* **2012**, *3*, 699.
(10) Wu, T. R.; Ding, G. Q.; Shen, H. J.; Wang, H. M.; Sun, L.; Jiang, D.; Xie, X. M.; Jiang, M. H. *Adv. Funct. Mater.* **2013**, *23*, 198.
(11) Song, H. S.; Li, S. L.; Miyazaki, H.; Sato, S.; Hayashi, K.; Yamada, A.; Yokoyama, N.; Tsukagoshi, K. *Sci. Rep.* **2012**, *2*, 337.
(12) Huang, P. Y.; Ruiz-Vargas, C. S.; van der Zande, A. M.; Whitney, W. S.; Levendorf, M. P.; Kevek, J. W.; Garg, S.; Alden, J. S.; Hustedt, C. J.; Zhu, Y.; Park, J.; McEuen, P. L.; Muller, D. A. *Nature* **2011**, *469*, 389.
(13) Yu, Q.; Jauregui, L. A.; Wu, W.; Colby, R.; Tian, J.; Su, Z.; Cao, H.; Liu, Z.; Pandey, D.; Wei, D.; Chung, T. F.; Peng, P.; Guisinger, N. P.; Stach, E. A.; Bao, J.; Pei, S. S.; Chen, Y. P. *Nat. Mater.* **2011**, *10*, 443.
(14) Mehdipour, H.; Ostrikov, K. *ACS Nano* **2012**, *6*, 10276.
(15) Hayashi, K.; Sato, S.; Ikeda, M.; Kaneta, C.; Yokoyama, N. *J. Am. Chem. Soc.* **2012**, *134*, 12492.
(16) Wofford, J. M.; Nie, S.; McCarty, K. F.; Bartelt, N. C.; Dubon, O. D. *Nano Lett.* **2010**, *10*, 4890.
(17) Wood, J. D.; Schmucker, S. W.; Lyons, A. S.; Pop, E.; Lyding, J. W. *Nano Lett.* **2011**, *11*, 4547.
(18) Chen, H.; Zhu, W. G.; Zhang, Z. Y. *Phys. Rev. Lett.* **2010**, *104*, 186101.
(19) Zhang, W. H.; Wu, P.; Li, Z. Y.; Yang, J. L. *J. Phys. Chem. C* **2011**, *115*, 17782.
(20) Riikonen, S.; Krasheninnikov, A. V.; Halonen, L.; Nieminen, R. M. *J. Phys. Chem. C* **2012**, *116*, 5802.
(21) Xu, L. S.; Jin, Y. K.; Wu, Z. F.; Yuan, Q.; Jiang, Z, Q.; Ma, Y. S.; Huang, W. X. *J. Phys. Chem. C* **2013**, *117*, 2952.
(22) Gao, J. F.; Yip, J.; Zhao, J. J.; Yakobson, B. I.; Ding, F. *J. Am. Chem. Soc.* **2011**, *133*, 5009.
(23) Zangwill, A.; Vvedensky, D. D. *Nano Lett.* **2011**, *11*, 2092.
(24) Wang, B.; Ma, X. F.; Caffio, M.; Schaub, R.; Li, W. X. *Nano Lett.* **2011**, *11*, 424.
(25) Cui, Y.; Fu, Q.; Zhang, H.; Bao, X. H. *Chem. Commun.* **2011**, *47*, 1470.
(26) Yuan, Q. H.; Gao, J. F.; Shu, H. B.; Zhao, J. J.; Chen, X. S.; Ding, F. *J. Am. Chem. Soc.* **2012**, *134*, 2970.
(27) Loginova, E.; Bartelt, N. C.; Feibelman, P. J.; McCarty, K. F. *New J. Phys.* **2008**, *10*, 093026.
(28) Wassei, J. K.; Mecklenburg, M.; Torres, J. A.; Fowler, J. D.; Regan, B. C.; Kaner, R. B.; Weiller, B. H. *Small* **2012**, *8*, 1415.
(29) Wesep, R. G.; Chen, H.; Zhu, W. G.; Zhang, Z. Y. *J. Chem. Phys.* **2011**, *134*, 171105.
(30) Wu, P.; Zhang, W. H.; Li, Z. Y.; Yang, J. L.; Hou, J. G. *J. Chem. Phys.* **2010**, *133*, 071101.
(31) Wang, L.; Zhang, X. Y.; Chan, L. W.; Yan, F.; Ding, F. *J. Am. Chem. Soc.* **2013**, *135*, 4476.
(32) Lu, J.; Yeo, P. S. E.; Gan, C. K.; Wu, P.; Loh, K. P. *Nat. Nanotechnol.* **2011**, *6*, 247.
(33) Mattevi, C.; Kim, H.; Chhowalla, M. *J. Mater. Chem.* **2011**, *21*, 3324.
(34) Rasool, H. I.; Song, E. B.; Mecklenburg, M.; Regan, B. C.; Wang, K. L.; Weiller, B. H.; Gimzewski, J. K. *J. Am. Chem. Soc.* **2011**, *133*, 12536.
(35) Rasool, H. I.; Song, E. B.; Allen, M. J.; Wassei, J. K.; Kaner, R. B.; Wang, K. L.; Weiller, B. H.; Gimzewski, J. K. *Nano Lett.* **2011**, *11*, 251.
(36) Gao, L.; Guest, J. R.; Guisinger, N. P. *Nano Lett.* **2010**, *10*, 3512.
(37) Cho, J.; Gao, L.; Tian, J. F.; Cao, H. L.; Wu, W.; Yu, Q. K.; Yitamben, E. N.; Fisher, B.; Guest, J. R.; Chen, Y. P.; Guisinger, N. P. *ACS Nano* **2011**, *5*, 3607.
(38) Nie, S.; Wofford, J. M.; Bartelt, N. C.; Dubon, O. D.; McCarty, K. F. *Phys. Rev. B* **2011**, *84*, 155425.
(39) Ago, H.; Ogawa, Y.; Tsuji, M.; Mizuno, S.; Hibino, H. *J. Phys. Chem. Lett.* **2012**, *3*, 2228.
(40) Zhu, Y.; Wyrick, J.; Cohen, K. D.; Magnone, K. M.; Holzke, C.; Salib, D.; Ma, Q.; Sun, D.; Bartels, L. *J. Phys.: Condens. Matter* **2012**, *24*, 354005.
(41) Stipe, B. C.; Rezaei, M. A.; Ho, W. *Science* **1998**, *280*, 1732.
(42) Dougherty, D. B.; Maksymovych, P.; Lee, J.; Yates, J. T., Jr. *Phys. Rev. Lett.* **2006**, *97*, 236806.
(43) Koerts, T.; Deelen, M. J. A. G.; Santen, R. A. *J. Catal.* **1992**, *138*, 101.
(44) Xu, Y. D.; Bao, X. H.; Lin, L. W. *J. Catal.* **2003**, *216*, 386.
(45) Banhart, F.; Kotakoski, J.; Krasheninnikov, A. V. *ACS Nano* **2011**, *5*, 26.
(46) Ugeda, M. M.; Fernández-Torre, D.; Brihuega, I.; Pou, P.; Martínez-Galera, A. J.; Pérez, R.; Gómez-Rodríguez, J. M. *Phys. Rev. Lett.* **2011**, *107*, 116803.
(47) Starodub, E.; Maier, S.; Stass, I.; Bartelt, N. C.; Feibelman, P. J.; Salmeron, M.; McCarty, K. F. *Phys. Rev. B* **2009**, *80*, 235422.
(48) Barreiro, A.; Börrnert, F.; Avdoshenko, S. M.; Rellinghaus, B.; Cuniberti, G.; Rümmeli, M. H.; Vandersypen, L. M. K. *Sci. Rep.* **2013**, *3*, 1115.
(49) Chen, J. H.; Shi, T. W.; Cai, T. C.; Xu, T.; Sun, L. T.; Wu, X. S.; Yu, D. P. *Appl. Phys. Lett.* **2013**, *102*, 103107.
(50) Jacobson, P.; Stöger, B.; Garhofer, A.; Parkinson, G. S.; Schmid, M.; Caudillo, R.; Mittendorfer, F.; Redinger, J.; Diebold, U. *J. Phys. Chem. Lett.* **2012**, *3*, 136.
(51) Karoui, S.; Amara, H.; Bichara, C.; Ducastelle, F. *ACS Nano* **2010**, *4*, 6114.
(52) Niu, T. C.; Zhou, M.; Zhang, J. L.; Feng, Y. P.; Chen, W. *J. Phys. Chem. C* **2013**, *117*, 1013.
(53) Huang, Y. L.; Lu, Y.; Niu, T. C.; Huang, H.; Kera, S.; Ueno, N.; Wee, A. T.; Chen, W. *Small* **2012**, *8*, 1423.
(54) Kresse, G.; Hafner, J. *Phys. Rev. B* **1993**, *47*, 558.
(55) Kresse, G.; Furthmuller, J. *Phys. Rev. B* **1996**, *54*, 11169.
(56) Perdew, J. P.; Burke, K.; Ernzerhof, M. *Phys. Rev. Lett.* **1996**, *77*, 3865.
(57) Kresse, G.; Joubert, D. *Phys. Rev. B* **1999**, *59*, 1758.
(58) Tersoff, J.; Hamann, D. R. *Phys. Rev. Lett.* **1983**, *50*, 1998.